Geospatial and Earth System Science
An International Triannual Scientific Journal

e-ISSN: 3139-549X | Vol. 1 | No. 2 | Page Nos. 52 – 66 | October 2026

Original Research Paper | https://www.maned.org/journals | **Open Access Journal**

Mapping Coastal Vulnerability in the Indian Sundarbans: An Integrated GIS and DEM-Based Assessment of Land Cover Change and Sea-Level Rise Inundation in South 24 Parganas District, West Bengal

Prahallad Barman[1]*, Rahul Debnath[2], Moumita Kisku[3]

[1,2] Department of Geography, University of Madras, Guindy Campus, Chennai-600025, Tamil Nadu, India

[1]ORCID: https://orcid.org/0009-0007-7098-1974

[2]ORCID: https://orcid.org/0009-0006-7671-4415

[3]Department of Remote Sensing & GIS, Vidyasagar University, Midnapore, West Bengal – 721102, India

[3]ORCID: https://orcid.org/0009-0001-9208-8323

*Corresponding Author: Prahallad Barman; prahalladbarman2002@gmail.com

Abbreviation: GESS
Website: www.maned.org/journals

Received: 10-08-2026
Revised: 20-09-2026
Accepted: 27-09-2026

Key Words:

CVI; LULC Change Detection; DEM-Based Inundation Modelling; Mangrove Ecosystem Dynamics; Sea-Level Rise

Copyright: © 2026 by the authors
Licensee: ManEd Research Foundation
This article is an open access article distributed under the terms and conditions of the Creative Commons Attribution (CC BY 4.0) license.

ABSTRACT

The Indian Sundarbans, where the Ganges–Brahmaputra delta meets the Bay of Bengal, ranks among the most ecologically fragile and socially exposed coastal landscapes in the world. This study presents an integrated coastal vulnerability assessment of the South 24 Parganas district of West Bengal, combining remote sensing, GIS, pre-classified land use/land cover (LULC) data, and elevation-based flood modelling across three reference years — 2017, 2021 and 2025. Three linked objectives guided the work: building a Coastal Vulnerability Index (CVI) from elevation, slope and land-cover inputs through a weighted overlay in Google Earth Engine; tracking land-cover change across the three years using the Dynamic World product; and simulating flood extent and depth under three sea-level scenarios (S0: 2.8 m, S1: 3.3 m, S2: 3.8 m) using a digital elevation model. By 2025, Low (27.67%) and Moderate (24.02%) classes dominated the CVI map, while Very High vulnerability still covered 12.50 percent of the area (960.82 km²). LULC change detection found that 17.95 percent of the district (1,376.95 km²) shifted category at least once between 2017 and 2025. Flood modelling placed 21.09 percent of the district (1,617.02 km²) within reach of extreme high tides today, rising to 36.23 percent (2,778.01 km²) once 0.5–1.0 m of additional sea-level rise is factored in. Together, these results offer a practical evidence base for coastal adaptation planning and disaster risk reduction in one of the world's most climate-exposed deltas.

INTRODUCTION

Coastal zones worldwide face growing strain from climate variability, rising seas and expanding settlement. Deltas and estuaries are especially exposed because their land sits close to sea level, their sediments shift constantly, and they support some of the highest population densities on the planet. The Indian Sundarbans, spanning roughly 9,630 km² on the Indian side of the Ganges–Brahmaputra–Meghna delta, is a case in point: simultaneously one of the richest coastal ecosystems on Earth and one of the most exposed to climate-driven hazards.

The region holds UNESCO World Heritage status, shelters the last significant wild Bengal Tiger population, hosts the largest unbroken mangrove belt on Earth, and supports around 4.5 million people dependent on its ecosystem services. Mangroves of this kind buffer coastlines against storm surges by dissipating wave energy (Kathiresan & Rajendran, 2005) and support broader coastal resilience under a warming climate (Alongi, 2008). This concern is not unique to the Sundarbans — deltas generally rank among the most at-risk landforms worldwide (Tessler et al., 2015), and tens of millions more people are projected to face

coastal flooding by mid-century as seas rise and coastal populations grow (Neumann et al., 2015).

The application of Geographic Information Systems (GIS) has further enhanced groundwater quality studies by enabling spatial analysis and visualization of contamination patterns. GIS-based approaches help in identifying high-risk zones and understanding the spatial variability of groundwater quality parameters, thereby supporting effective water resource management (Srinivasamoorthy et al., 2014).

Vulnerability here stems from several compounding factors. The delta comprises about 102 islands laced with tidal creeks, and relative sea-level rise has been measured at roughly 3.14 mm/yr — well above the global average of 1.8 mm/yr — driven by land subsidence, compaction and reduced sediment supply. Severe cyclones, including Aila (2009), Bulbul (2019), Amphan (2020) and Yaas (2021), have repeatedly breached embankments, flooded farmland and displaced communities. The mangrove belt that would normally buffer the coast is itself under pressure from illegal felling and the steady conversion of forest and cropland to shrimp and fish ponds, a shift documented across the Indian Sundarbans Biosphere Reserve over the past two decades (Giri et al., 2022). Most residents work in farming, fishing or forestry, placing them in direct contact with these hazards, while earthen embankments — often the only barrier between a settlement and the sea — remain the primary defence. The Coastal Vulnerability Index, first formulated by the U.S. Geological Survey, offers a structured way to combine physical and geomorphic variables into one comparable score, and GIS and remote sensing make this kind of analysis feasible across a large, otherwise hard-to-survey delta.

This study builds such an assessment for South 24 Parganas across 2017, 2021 and 2025, through four aims: constructing a spatially explicit CVI from elevation, slope and land-cover inputs; quantifying land-cover change across the three years; modelling flood extent and depth under three sea-level rise scenarios; and synthesising these three strands into a single interpretation of vulnerability drivers and flood risk.

The geographic focus is the 7,668.06 km² South 24 Parganas district, spanning 19 Community Development Blocks and roughly 102 islands. The study relies entirely on open satellite products — the Dynamic World land-cover dataset and the Copernicus GLO-30 DEM — processed through Google Earth Engine. Field validation and socio-economic indicators fall outside this scope and are flagged as directions for future work.

STUDY AREA

The Indian Sundarbans occupies the southern edge of the Ganges–Brahmaputra delta, one of the largest and most active deltaic systems on Earth. The study area is the South 24 Parganas district of West Bengal, containing the entire Indian portion of the Sundarbans. It lies between 21°31'N–22°30'N and 88°03'E–89°07'E, along the northern Bay of Bengal margin, covering 7,668.06 km² across 19 Community Development Blocks and around 102 islands, with roughly 210 km of coastline threaded inland by a dense network of tidal creeks and channels.

The district is bordered north by mainland South 24 Parganas, south by the Bay of Bengal, west by the Muriganga estuary, and east by Bangladesh; the Bangladesh Sundarbans (roughly 6,017 km²), with its own distinct mangrove wildlife (Aziz & Paul, 2015), forms the eastern continuation of the delta but falls outside this study. Notable blocks include Sagar Island, Gosaba, Patharpratima, Kultali, Hingalganj, Basirhat, Canning, Kakdwip and Namkhana. Historical map and satellite comparisons show the Hooghly (Hugli) estuary's banks and islands shifting substantially over the twentieth century (Bandyopadhyay et al., 2004), and more recent bank-line analyses confirm this erosion–accretion process is ongoing rather than historical (Anam, Al Jabir, & Hasan, n.d.).

Physiographically, this is a tide-dominated, wave-influenced delta with a two-to-four-metre tidal range. Ground elevation rarely exceeds two to three metres above mean sea level, leaving the landscape highly exposed to tidal flooding and storm surges. Sagar Island, at the mouth of the Hooghly estuary, is the largest island and one of the most exposed to cyclonic surges. The western blocks — Namkhana, Sagar and Kakdwip — face open-ocean wave energy and erode faster; radar-based studies have measured coastline retreat of up to 200 m per year in comparably exposed stretches of the delta (Pettorelli et al., 2013). The more sheltered eastern blocks accumulate sediment and support greater mangrove growth. Soils are predominantly fine-grained alluvial and silty clays that destabilise when saturated, contributing to compaction-driven subsidence and the locally elevated rate of relative sea-level rise.

The climate is tropical monsoon, with 1,600–1,800 mm of annual rainfall, three-quarters of it falling June to September. The pre-monsoon (March–May) brings the highest cyclone risk in the Bay of Bengal, while October–December marks a secondary cyclone season. The forest supports 64 mangrove and associated species, including Heritiera fomes (Sundari),

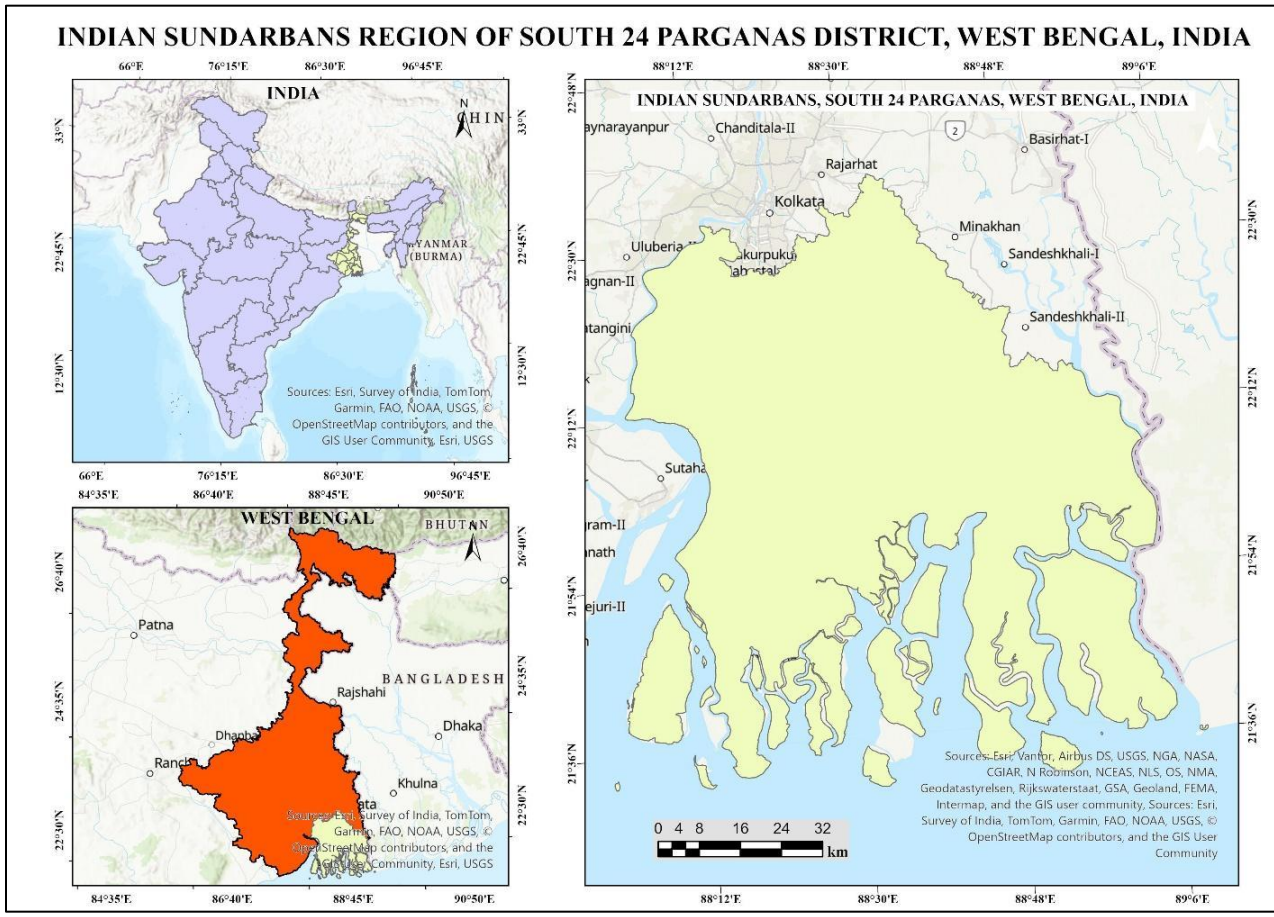


Fig.1: Location of the study area — the Indian Sundarbans within South 24 Parganas district, West Bengal, shown against the national and state context.

Excoecaria agallocha, Avicennia marina and Rhizophora mucronata. The Sundari tree, for which the Sundarbans is named, has declined sharply from top-dying disease and rising salinity — a loss that weakens the coastal protection the mangrove belt provides. Multi-decadal Landsat-based assessments confirm this decline is part of a sustained, basin-wide reduction in mangrove extent and vigour since 2000 rather than a local anomaly (Samanta et al., 2021). Salinity is lower in the west, near the Hooghly estuary (5–10 ppt in the monsoon, 15–25 ppt in the dry season), than in the less freshwater-fed central and eastern sectors (10–20 ppt monsoon, 25–35 ppt dry season); reduced upstream discharge has pushed salinity higher over time, stressing both mangrove health and farm productivity.

METHODOLOGY

Data Source

Dataset choice was guided by three criteria: full coverage of the 7,668.06 km² study area, availability across all three benchmark years, and open access via cloud platforms. All processing used Google Earth Engine (GEE), summarised in Table 1.

The Dynamic World product (Brown et al., 2022) delivers near-real-time land cover at 10 m resolution using a deep-learning model trained on Sentinel-2 imagery, with nine classes: Water, Trees, Flooded Vegetation, Crops, Built Area, Bare Ground, Snow/Ice, Clouds and Rangeland. Annual median composites were built from cloud-free Sentinel-2 scenes for each benchmark year, avoiding bias from any single date.

The Copernicus DEM (GLO-30) is derived from TanDEM-X radar interferometry at roughly 30 m resolution with ~1.0 m vertical accuracy for low-relief coastal terrain — an improvement over the older SRTM DEM for a delta this flat. It was void-filled with a 3×3 focal mean filter and clipped to the study boundary before use.

Data Pre-processing

The Dynamic World layer was filtered to exclude pixels with over 20 percent cloud probability, composited annually, and resampled to the DEM grid via bilinear interpolation. Each class

was then assigned an integer vulnerability rank (1–5) The DEM was gap-filled a 3 x 3 focal mean Kemel.

Slope computed in degrees via ee.Terrain.slope, and both layers reclassified into five vulnerability tiers using the thresholds in Tables 2 and 3. All layers were reprojected to WGS 84 / UTM Zone 45N at a common 30 m pixel size.

Table 1. Primary datasets used in this study.

Dataset	Source	Resolution	Years Used
Pre-classified LULC (Dynamic World)	Google Earth Engine / Dynamic World	10 m	2017, 2021, 2025
Copernicus DEM (GLO-30)	Copernicus / TanDEM-X	~30 m (1 arc-second)	All years
Study area boundary (South 24 Parganas)	GEE asset (user-uploaded)	Vector	All years
Tidal gauge data	NIOT /IMD	Station-level	2017–2025
Census data	Census of India	Block-level	2011 (reference)

Analytical Framework

The overall workflow proceeds through three parallel analytical streams that converge into a single integrated interpretation. Data collection and pre-processing feed into CVI modelling, LULC change detection, and DEM-based flood simulation; the outputs of these three streams are then overlaid and cross-tabulated, checked against available reference information, and interpreted jointly to produce vulnerability maps, a change-detection report and inundation maps, culminating in the conclusions presented in this document.

The CVI stream combines elevation, slope and land-cover vulnerability ranks using the weighted-overlay procedure detailed in Section 3.4. The LULC change-detection stream compares annual composites pixel by pixel across three intervals to flag where land cover changed. The inundation stream applies a static bathtub model to the DEM, marking any pixel below a given scenario's water level as flooded provided it is hydrologically connected to the open coast, determined through connected-component analysis.

Coastal Vulnerability Index (CVI) Formulation

The Coastal Vulnerability Index is a composite score that expresses the relative physical exposure of a stretch of coastline to hazards such as sea-level rise, tidal flooding and erosion. Originally proposed by the USGS (Thieler & Hammar-Klose, 2000), it combines several geomorphic and land-cover inputs into one ranked measure. In this study, the index was computed as:

CVI = (0.4 × Elevation Rank) + (0.3 × Slope Rank) + (0.3 × LULC Rank)

Elevation carries the greatest weight because it is the single strongest determinant of flood exposure in a delta this flat; slope and land cover are weighted equally behind it, reflecting their shared, if secondary, role in shaping how quickly floodwater spreads and how much natural or engineered protection a given area retains.

Table 2. Elevation classification used in CVI computation.

Elevation (m above MSL)	Vulnerability Class	CVI Rank
> 4.0	Very Low	1
3.0 – 4.0	Low	2
2.0 – 3.0	Moderate	3
1.0 – 2.0	High	4
< 1.0	Very High	5

Table 3. Slope classification used in CVI computation.

Slope (degrees)	Vulnerability Class	CVI Rank
> 4.0	Very Low	1
3.0 – 4.0	Low	2
2.0 – 3.0	Moderate	3
1.0 – 2.0	High	4
< 1.0	Very High	5

Elevation was drawn directly from the Copernicus DEM. Because most of the study area lies below three metres above mean sea level, with the southern islands frequently under one metre, the elevation surface shows a gentle rise toward the north and progressively lower ground toward the coast.

Slope was computed from the same void-filled DEM. As expected for a low-relief delta, slope values across almost the entire study area fall below one degree, offering negligible topographic resistance to inland flood propagation.

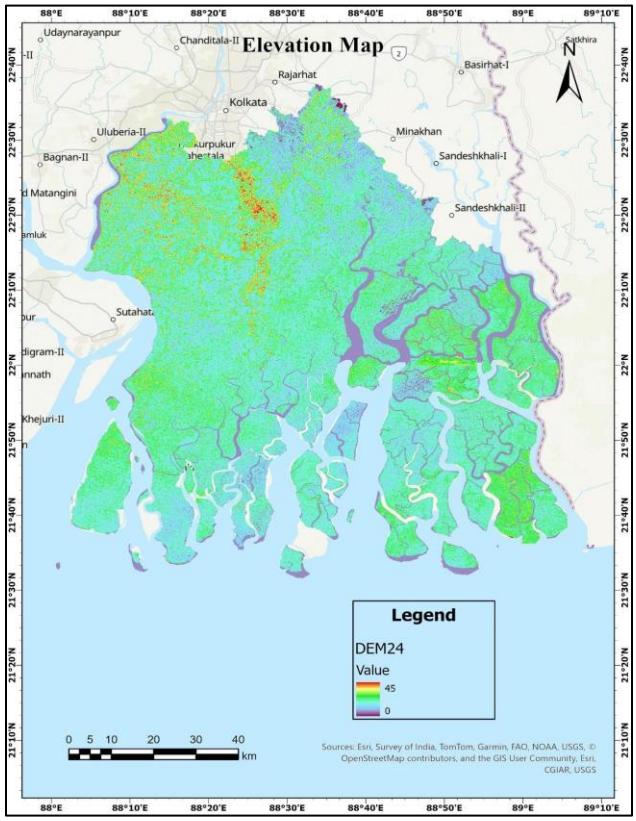


Fig. 2: Elevation surface of the Indian Sundarbans derived from the Copernicus GLO-30 DEM.

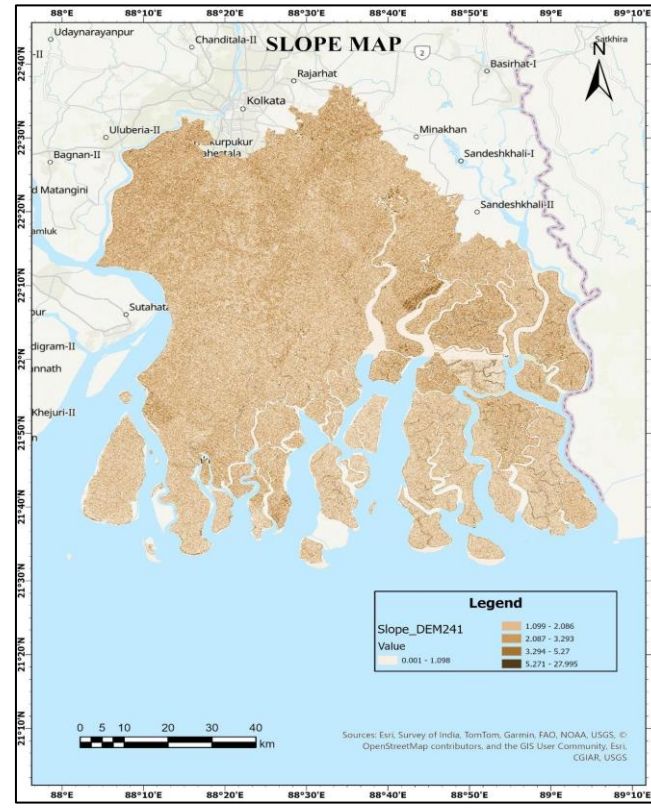


Fig. 3: Slope surface of the Indian Sundarbans study area, confirming the near-uniform flatness of the terrain, particularly across the southern islands.

Table 4. LULC vulnerability reclassification applied to Dynamic World classes.

LULC Class	Dynamic World Value	Vulnerability Rank	Rationale
Dense Vegetation / Mangrove	1 (Trees)	1 — Very Low	Attenuates wave energy; roots stabilise sediment
Sparse / Flooded Vegetation	2 (Flooded Veg.)	2 — Low	Partial protection; seasonally inundated
Rangeland / Scrub	8 (Rangeland)	2 — Low	Degraded cover; limited protective value
Agriculture / Crops	3 (Crops)	3 — Moderate	Productive land, moderately exposed to tidal flooding
Bare Land / Mudflat	5 (Bare Ground)	4 — High	Active erosion; no vegetative protection
Built-up / Settlement	4 (Built Area)	5 — Very High	High exposure of population and assets
Water Body / Tidal Channel	0 (Water)	5 — Very High	Represents baseline inundation and maximum flood risk

The three ranked layers — elevation, slope and land cover — were combined pixelwise in Google Earth Engine at 30 m resolution using the weighted formula above, and the resulting continuous score was grouped into five classes for mapping: Very Low (1.0–1.8), Low (1.8–2.6), Moderate (2.6–3.4), High (3.4–4.2) and Very High (4.2–5.0).

Land Use / Land Cover Change Detection Method

Change detection relied on a straightforward binary comparison: for each pixel, the land-cover class recorded in one benchmark year was compared against the class recorded in another. Any pixel whose class differed between the two dates was flagged as 'Changed'; all others were marked 'No Change'. This was carried out for three intervals — 2017–2021, 2021–2025 and the full 2017–2025 span — using the class scheme in Table 6 of the Results section. Earlier LULC studies of the Indian Sunderbans have applied comparably direct classification-comparison techniques to track coastal land change (Datta & Deb, 2012), while more elaborate approaches such as multi-layer-perceptron Markov-chain modelling have been used elsewhere in the delta to additionally project future land-cover trajectories (Sardar & Samadder, 2021); the binary method adopted here trades that predictive capability for simplicity and transparency. Because it is directionally blind, it captures both degradation (for example, mangrove converting to bare ground) and recovery (bare ground regaining vegetation) under the same 'Changed' label, so the resulting percentages describe the overall magnitude of land-cover dynamism rather than decline specifically.

DEM-Based Inundation Modelling Method

Inundation was modelled using a static 'bathtub' approach applied to the void-filled Copernicus DEM. Three water-level scenarios were tested, aligned with the IPCC AR6 SSP2-4.5 intermediate emissions pathway: S0 at 2.80 m, representing today's extreme high tide; S1 at 3.30 m, approximating conditions around 2050 with half a metre of additional sea-level rise; and S2 at 3.80 m, representing an end-of-century condition with a full metre of rise. For each scenario, every pixel with an elevation below the scenario threshold was flagged as flooded, provided it was hydrologically connected to the open coast through a connected-component analysis rather than being an isolated low-lying depression. Flood depth at each flooded pixel was then computed as the scenario water level minus the pixel's DEM elevation. This bathtub-style approach follows the same logic used in earlier shoreline and inundation studies applying satellite-derived elevation and imagery to Indian and Bangladeshi delta coastlines (Ghosh, Kumar, & Roy, 2014), though it necessarily simplifies the more complex tidal hydrodynamics that govern actual flood propagation through the Sundarbans' channel network (Das, 2021).

RESULTS

Coastal Vulnerability Index

The 2017 CVI map shows a vulnerability pattern shaped chiefly by mangrove distribution and low-lying terrain along the southern coastal blocks. Areas of Very High vulnerability cluster in the southern tip of Sagar Island, the western shoreline of Gosaba block, and the southwestern coast of Patharpratima block. In this baseline year, Low vulnerability was the single largest class at 2,034.68 km² (26.53%), suggesting a relatively broad extent of land was still buffered by sparse mangrove and cropland.

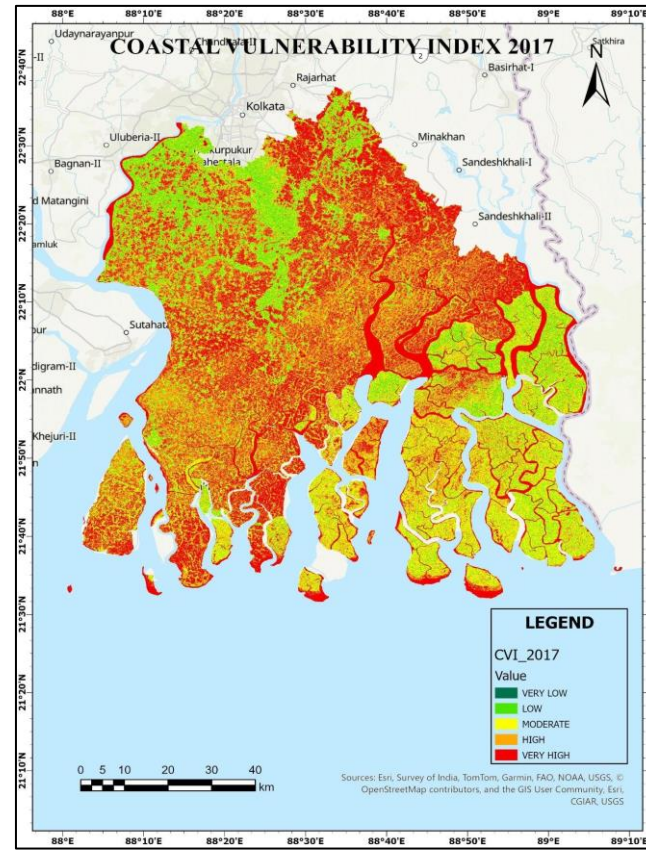


Fig.4: Coastal Vulnerability Index map for 2017, classified from Very Low to Very High across the 7,668.06 km² study area.

The 2021 map shows a modest shift relative to 2017. The Very Low class grew slightly, from 1,177.41 km² to 1,202.58 km², which may reflect a short-lived rebound of sparse vegetation in the aftermath of Cyclone Amphan (May 2020). The High and Very High classes contracted marginally over the same period, though this could equally reflect short-term

classification noise during the post-cyclone recovery window rather than a genuine reduction in physical exposure.

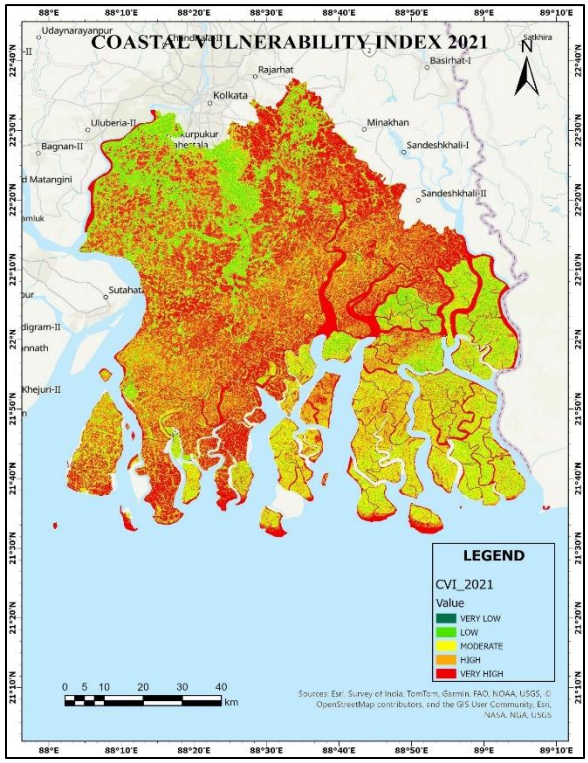


Fig. 5: Coastal Vulnerability Index map for 2021, showing a slight reduction in Very High CVI zones relative to 2017.

By 2025, the Very Low class had grown to 1,267.39 km² (16.49%) and the Low class to 2,127.16 km² (27.67%), together accounting for 44.16 percent of the district. Even so, the combined High and Very High classes still covered 31.58 percent of the study area — 2,427.51 km² — indicating that nearly a third of South 24 Parganas remains under substantial physical exposure.

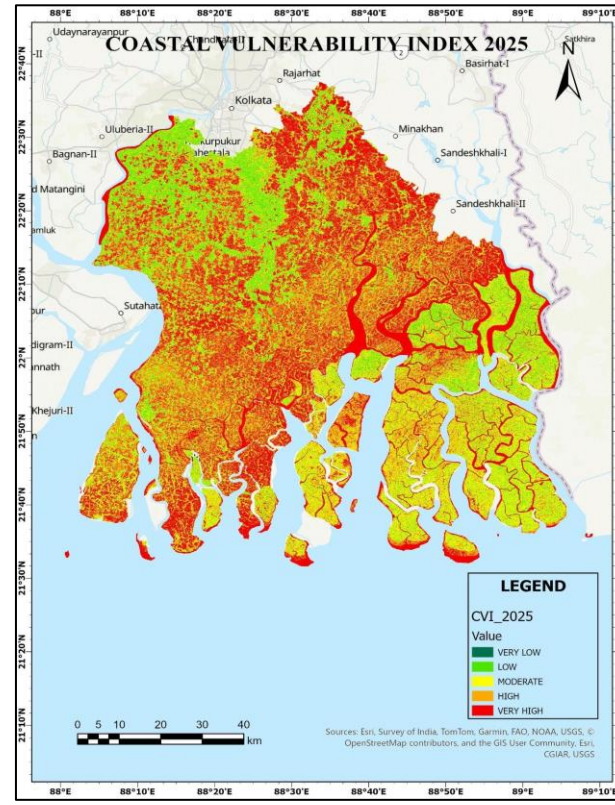


Fig. 6: Coastal Vulnerability Index map for 2025; High and Very High classes together cover 31.58% of the study area (2,427.51 km²).

Table 5. CVI area distribution across the three benchmark years.

CVI Class	2017 Area (km²)	2021 Area (km²)	2025 Area (km²)	% (2025)
Very Low (1)	1,177.41	1,202.58	1,267.39	16.49%
Low (2)	2,034.68	2,071.33	2,127.16	27.67%
Moderate (3)	1,917.75	1,916.34	1,846.00	24.02%
High (4)	1,531.16	1,512.20	1,466.69	19.08%
Very High (5)	1,007.06	965.60	960.82	12.50%
TOTAL	7,668.06	7,668.05	7,668.06	100%

The consistent total area across all three years (within rounding) confirms that the study boundary remained stable throughout, lending confidence to the area-based change statistics reported here. The modest decline in the High and Very High classes between 2017 and 2025 should not be read as a straightforward improvement in coastal resilience — it more likely reflects a mix of land-cover shifts producing offsetting vulnerability signals at the regional scale rather than a uniform recovery.

Land Use / Land Cover Change Detection

Classification maps for all three benchmark years were derived from the Dynamic World product, which offers 10 m resolution land cover generated through a deep-learning model applied to Sentinel-2 imagery (Brown et al., 2022). For the Sundarbans, the classes of greatest relevance are Trees (mangrove forest), Flooded Vegetation, Crops, Built Area, Bare Ground and Water.

Table 6. Dynamic World land cover classes and their coastal vulnerability role.

Class Value	Class Name	Coastal Vulnerability Role
0	Water	Tidal channels and open sea; baseline inundation
1	Trees / Mangrove	Natural wave attenuation and sediment trapping
2	Flooded Vegetation	Seasonally inundated; moderate-to-high exposure
3	Crops / Agriculture	Productive farmland; moderate exposure
4	Built Area / Settlement	High social exposure — population and assets at risk
5	Bare Ground / Mudflat	Active erosion surface; no vegetative protection
8	Rangeland / Scrub	Degraded or transitional cover; moderate-to-high exposure

Change detection was carried out as a binary comparison — changed versus unchanged — across three intervals: 2017–2021, 2021–2025 and the full 2017–2025 span. Because this approach does not distinguish the direction of change, the resulting figures capture both degradation (for example, mangrove loss) and recovery (regrowth on previously bare or cleared land) within the same 'Changed' category.

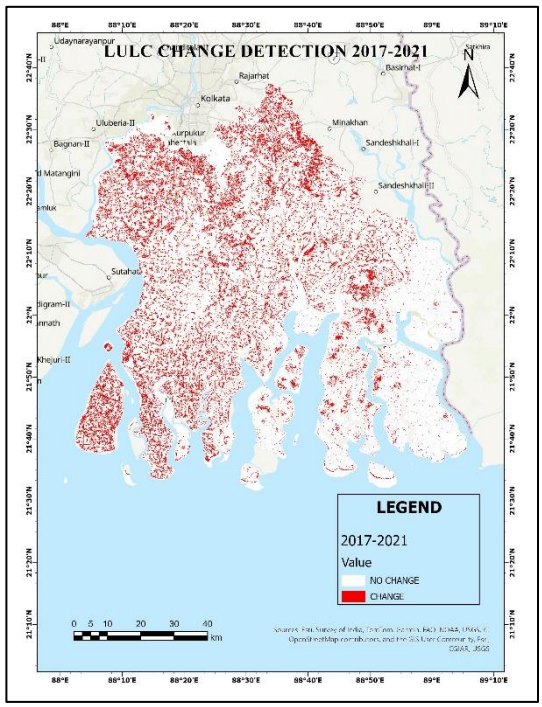


Fig.7: Binary land cover change map, 2017–2021. Changed area totals 1,236.85 km² (16.13%), concentrated in the southern coastal blocks and areas affected by Cyclone Amphan.

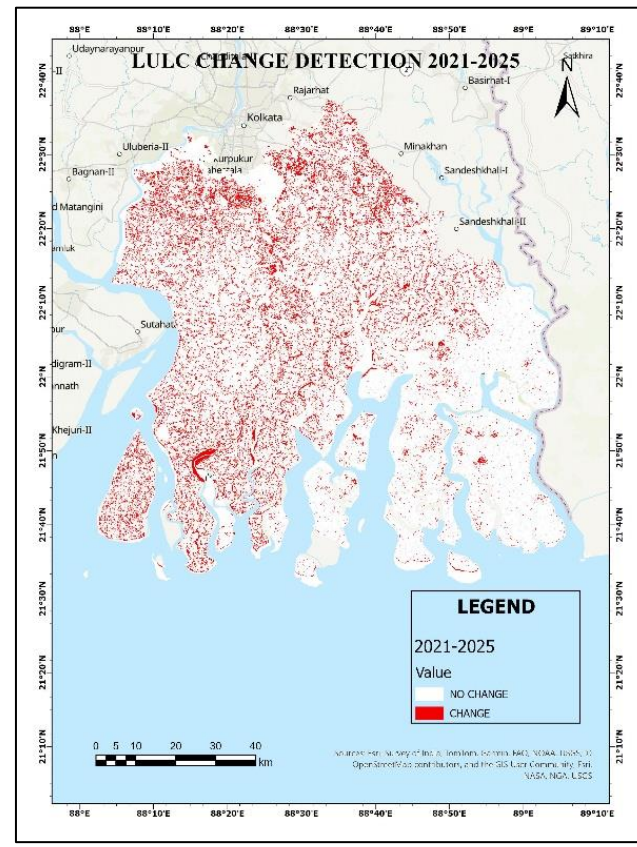


Fig. 8: Binary land cover change map, 2021–2025. Changed area totals 967.99 km² (12.62%), a lower rate consistent with post-cyclone landscape stabilization.

Across the full study period, 1,376.95 km² — 17.95 percent of the district — registered a detectable shift in land-cover class. The steepest rate of change, 16.13 percent (1,236.85 km²), fell

within the 2017–2021 window, overlapping with Cyclone Amphan in May 2020, which breached embankments,

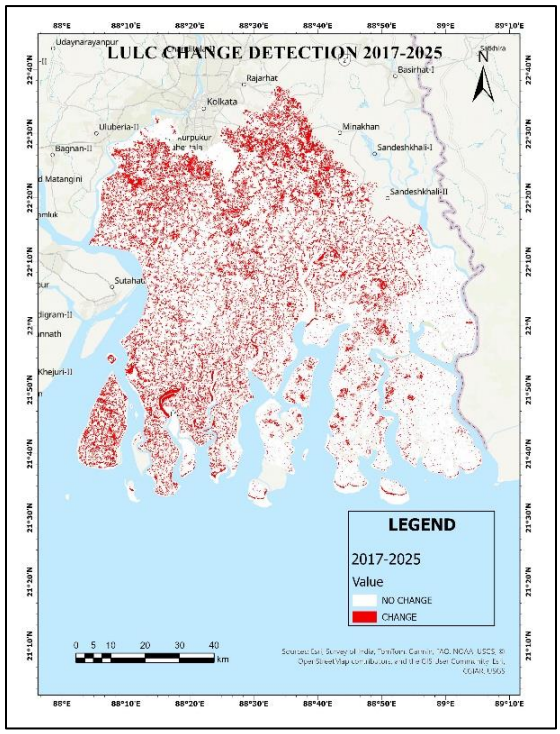


Fig. 9: Binary land cover change map for the full 2017–2025 period. Total changed area reaches 1,376.95 km² (17.95%), with persistent hotspots in Sagar Island, Gosaba and Patharpratima blocks

Table 7. Land cover change detection results by interval.

Period	No Change (km²)	Change (km²)	Change (%)
2017–2021	6,431.09	1,236.85	16.13%
2021–2025	6,699.95	967.99	12.62%
2017–2025	6,290.99	1,376.95	17.95%

flooded an estimated 1,500 km² of farmland, and damaged mangrove stands extensively. The following 2021–2025 period shows a markedly lower change rate of 12.62 percent, consistent with a degree of landscape recovery and stabilisation.

DEM-Based Inundation Modelling

Three flood scenarios were tested, aligned with the IPCC AR6 SSP2-4.5 pathway, as summarised in Table 8.

Under the S0 baseline, 1,617.02 km² — 21.09 percent of the study area — is already within reach of extreme high tidal conditions.

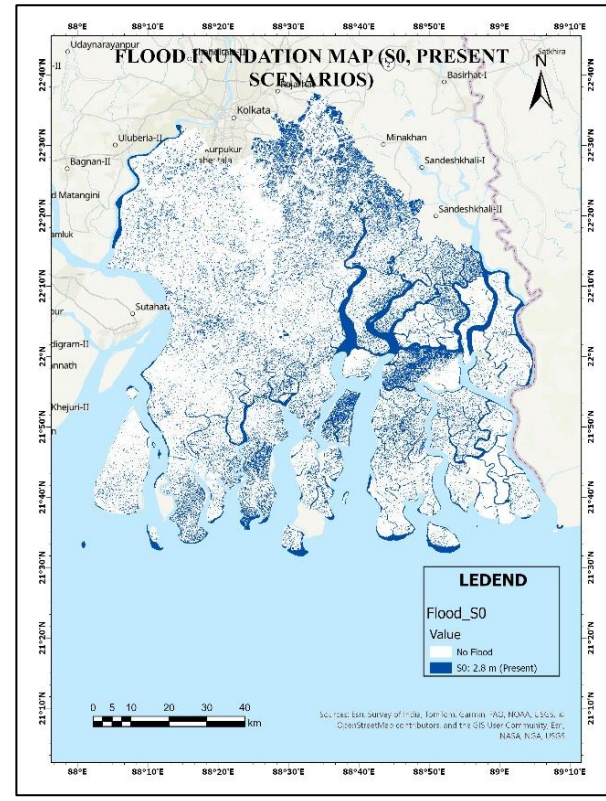


Fig. 10: (a). Flood inundation extent under scenario S0 (2.80 m, present-day). Flooded area = 1,617.02 km² (21.09%)

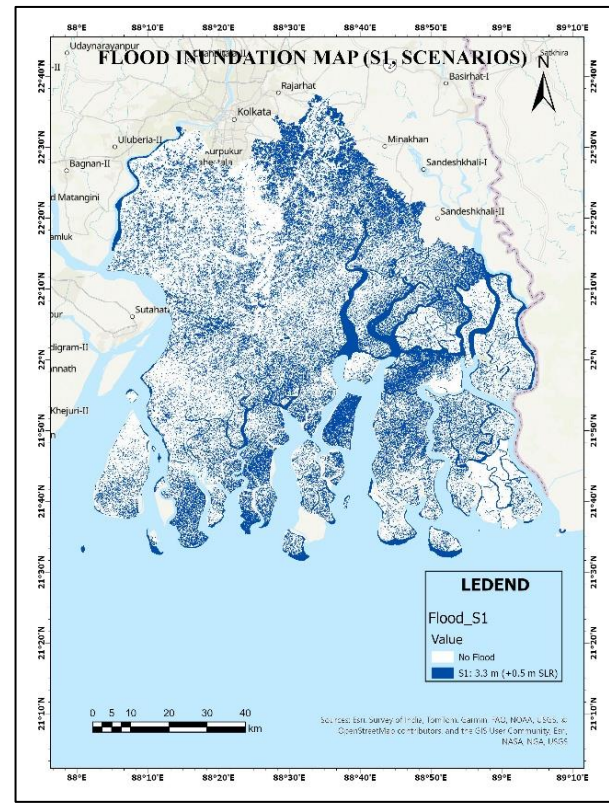


Fig. 10: (b). Flood inundation extent under scenario S1 (3.30 m, +0.5 m sea-level rise). Flooded area = 2,778.01 km² (36.23%).

Moving to S1, with half a metre of additional sea-level rise, the flooded area expands sharply to 2,778.01 km² (36.23%) — an 82 percent increase over the baseline and an additional 1,160.99 km² brought within the flood zone.

Scenario S2 produces an identical flood footprint to S1 — 2,778.01 km² (36.23%) — which points to a topographic plateau at this water-level increment given the 30 m resolution of the DEM: once the readily flooded low-lying land is inundated, the next tier of higher ground only submerges at a threshold beyond what S2 represents at this resolution.

Table 8. Flood scenario definitions.

Scenario	Water Level (m)	Basis	Approx. Return Period	Rationale
S0	2.80 m	Present Mean High Water Spring (MHWS)	Annual	Present-day extreme high tide; baseline inundation
S1	3.30 m	MHWS + 0.5 m sea-level rise	~25 years	Approximate 2050 condition under SSP2-4.5
S2	3.80 m	MHWS + 1.0 m sea-level rise	~100 years	Approximate end-of-century condition under SSP2-4.5

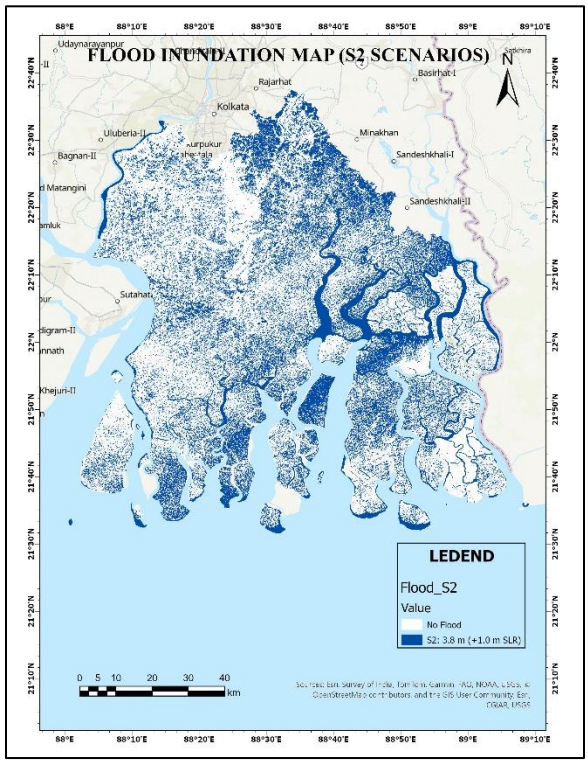


Fig. 10: (c). Flood inundation extent under scenario S2 (3.80 m, +1.0 m sea-level rise). Flooded area = 2,778.01 km² (36.23%), matching S1.

Flood depth maps add a further dimension by showing not just where water reaches but how deep it sits, computed as the scenario water level minus the DEM elevation at each flooded pixel. This distinction matters for damage assessment and infrastructure planning, since shallow flooding under half a metre carries very different consequences from flooding deeper than a metre and a half.

Table 9. Flood area under each sea-level scenario.

Scenario	Water Level (m)	Flood Area (km²)	% of Study Area
S0	2.80 m	1,617.02	21.09%
S1	3.30 m	2,778.01	36.23%
S2	3.80 m	2,778.01	36.23%

Table 10. Flood depth classification and typical impact.

Depth Range (m)	Severity
0 – 0.3 m	Low
0.3 – 0.8 m	Moderate
0.8 – 1.5 m	High
1.5 – 2.5 m	Very High
> 2.5 m	Extreme

Flood severity increases progressively with water depth, from minor impacts at 0–0.3 m to extreme damage and infrastructure failure above 2.5 m. Higher flood depths are associated with greater agricultural and settlement damage, structural impacts, and increasing requirements for evacuation and emergency response.

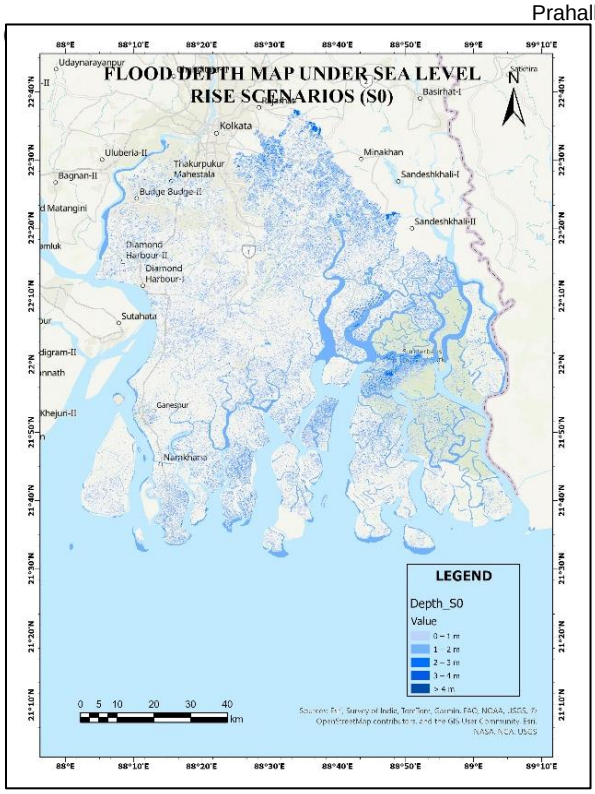


Fig. 11: Flood depth under scenario S0 (2.80 m). Depths range from 0–2.8 m, concentrated in tidal channels, mudflats and the lowest-lying coastal fringes

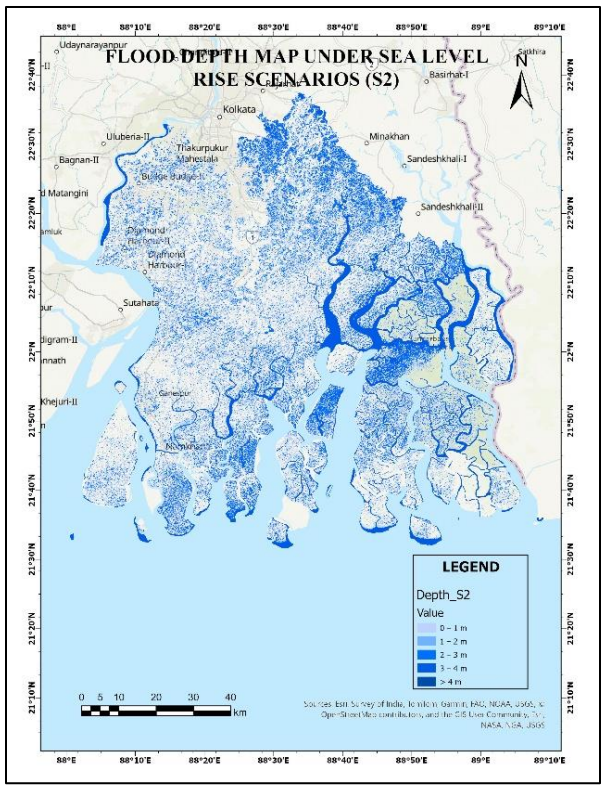


Fig. 12: Flood depth under scenario S1 (3.30 m). Flood depth extends further across agricultural lowlands in Sagar Island, Gosaba, Patharpratima and Hingalganj blocks.

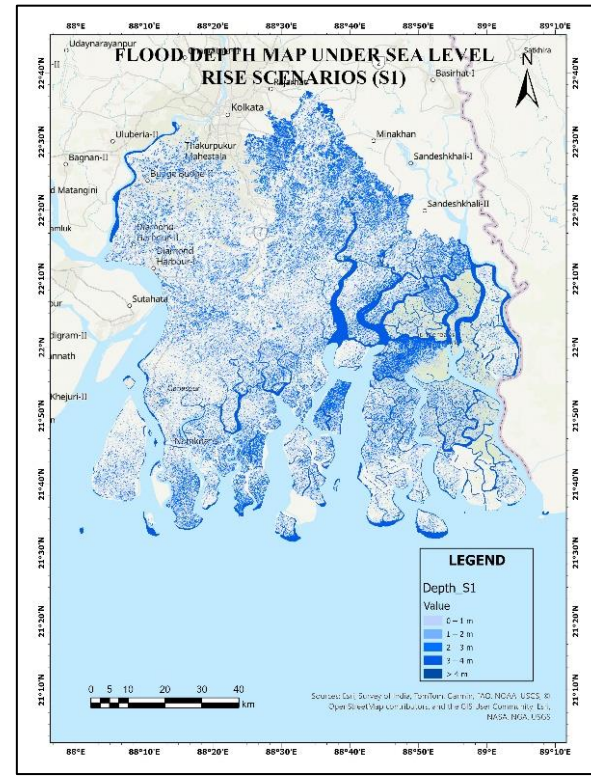


Fig. 13: Flood depth under scenario S2 (3.80 m). Maximum depths exceed 2.5 m across the lowest-lying tidal flats.

DISCUSSION

Interpreting the Combined

Together, the CVI trends, land-cover change patterns and flood modelling outputs point to a coastal system under sustained, spatially uneven pressure. Although the Very High CVI class edged down slightly, from 1,007.06 km² in 2017 to 960.82 km² in 2025, the combined High and Very High classes still cover 31.58 percent of the study area (2,427.51 km²) — a scale of exposure consistent with broader delta vulnerability trajectories under moderate-emissions futures.

At a regional scale, relative sea-level rise driven by a mix of global (eustatic) rise — projected at 0.3 to 0.6 m by 2100 under SSP2-4.5 pathways more broadly (Nicholls et al., 2021) — and local land subsidence, estimated at 1.2 to 2.4 mm per year from InSAR measurements across the Sundarbans (Biswas et al., 2020), is steadily eroding the effective freeboard of the low-lying islands. The inundation results make this concrete: 21.09 percent of the district is already flood-exposed under present extreme tides, and that share rises to 36.23 percent under conditions representative of roughly 2050. This is consistent with block-level land-loss figures reported for the Indian Sundarbans in the early 2000s, when roughly 5.5 km² of land was being lost to erosion each year even before the more recent run of major cyclones (Hazra & Samanta, 2016), and with

longer Landsat-based time series showing that erosion has generally outpaced accretion across the delta over the past several decades (Mahato, 2024).

How CVI, Land Cover and Flooding Relate to One Another

One of the clearer patterns to emerge from this study is the spatial overlap between high CVI scores, active land-cover change, and projected flood extent in the southern and western coastal blocks. Sagar Island, Gosaba, Patharpratima and Hingalganj consistently appear as hotspots across all three lines of analysis: they carry the largest share of Very High CVI pixels, the greatest magnitude of land-cover change between 2017 and 2025, and the largest projected flood footprints under the S1 and S2 scenarios.

Part of this overlap is built into the method, since the CVI formula assigns land cover a 30 percent weight. But the convergence observed here goes beyond that definitional link — it reflects a genuine feedback loop between ecological degradation and rising physical exposure. Where mangrove cover gives way to bare ground or aquaculture ponds, a shift also documented in long-term forest-cover surveys of the Indian Sundarbans (Nandy et al., n.d.) and in studies linking channel migration to mangrove loss along tidal banks (Ghosh, Kumar, & Langat, 2018), the natural wave attenuation and sediment-trapping functions mangroves provide are lost at the same time, directly raising shoreline vulnerability. The inundation results add a third layer: areas identified as Very High CVI in 2025 sit disproportionately below one metre above mean sea level, meaning they are already inundated under the S0 baseline — communities and farmland here are not just theoretically vulnerable but already flooding under present tidal conditions, with further expansion likely even under the most conservative sea-level rise projections considered.

Positioning These Findings Alongside Earlier Work

These results sit comfortably alongside earlier assessments of coastal vulnerability and land-cover change in the Indian Sundarbans. Biswas, Mondal and Ray (2020) reported InSAR-derived subsidence rates of 1.2 to 2.4 mm per year across the delta, a factor that compounds global sea-level rise and helps explain why relative sea-level rise here consistently exceeds the global mean. Separately, Mukhopadhyay and colleagues (2012) applied comparable remote-sensing methods to track shoreline change along the Puri coast, demonstrating that Earth Engine-based workflows of the kind used here translate well to other Indian coastal settings.

Kantamaneni and colleagues (2019), in their review of coastal vulnerability studies along the Indian coastline, noted that multi-parameter, multi-temporal assessments remain relatively rare in deltaic environments — a gap this study attempts to narrow by offering a three-year, three-objective assessment specific to the South 24 Parganas Sundarbans. More recent work reinforces this picture from different angles: Das and colleagues (2025) applied the InVEST coastal vulnerability model together with machine-learning validation across four decades of Sundarbans shoreline data and likewise found rising vulnerability over time, while Ghosh and Mistri (2023) documented substantial inter-village variation in cyclone vulnerability across the Matla–Bidya inter-estuarine area, underlining how uneven exposure can be even within a single sub-region. McLaughlin and Cooper (2010) argued more generally that multi-scale vulnerability tools are essential for practical coastal management, and the block-level resolution of the outputs presented here is intended to support exactly that kind of operational use.

The flood extents obtained in this study — 21.09 percent under S0 and 36.23 percent under S1/S2 — are somewhat more conservative than figures reported by studies using higher-resolution LiDAR-derived elevation data, which typically detect greater inundated area in ultra-low-relief deltaic terrain. This gap is expected given the 30 m resolution and associated vertical uncertainty of the Copernicus DEM, and the figures reported here should be read as a cautious lower bound on the true extent of inundation risk rather than an upper estimate. Comparable decadal shoreline and geomorphological change mapping elsewhere in West Bengal's coastal belt has reported similarly patchy, block-by-block variation in erosion and accretion rather than a single uniform trend (Rahman et al., n.d.), and openly published Sundarbans vulnerability datasets built through parallel weighted-index approaches (Ganguli, 2024) offer a useful basis for future cross-study comparison as more such assessments accumulate for this delta. It is also worth noting that the physical exposure captured by the CVI here is only part of the picture: livelihood-based vulnerability assessments in the Indian Sundarbans point to substantial variation in adaptive capacity between blocks that share similar physical exposure, driven by differences in income, asset ownership and access to alternative livelihoods (Sarkar et al., n.d.) — a social dimension this physically-focused study does not attempt to capture but which future integrated work should incorporate.

What These Results Mean for Planning

The environmental implications of these findings are substantial. Identifying 960.82 km² (12.50%) of the study area as Very High CVI in 2025 — with 2,427.51 km² (31.58%) falling into the combined High and Very High classes —

suggests that the natural protective capacity the Sundarbans ecosystem once offered is no longer sufficient to shield the current population from the climate hazards it now faces. The mangrove belt continues to deliver valuable ecosystem services, but it no longer covers enough of the coastline, at sufficient density, to meaningfully dampen storm surge or slow erosion in the areas that need it most. This is compounded by the seasonal sediment dynamics of the delta: work on sedimentation patterns in the wider Sundarbans forest has shown that the balance of deposition and erosion shifts markedly between monsoon and dry-season conditions, which means the protective capacity of any given stretch of mangrove is not constant through the year (Hale, Wilson, & Bomer, 2019). The scale of damage recorded after Cyclone Amphan — including embankment breaches and widespread inundation of farmland across South 24 Parganas (West Bengal SDMA, 2020) — offers a recent, concrete illustration of exactly the kind of event these vulnerability maps are intended to help anticipate.

For spatial planning and disaster risk reduction, the overlap identified flags clear priority zones: the southern shoreline of Sagar Island, the western coast of Gosaba block, the coastal fringe of Patharpratima block, and Hingalganj block in the eastern Sundarbans. These areas combine high CVI, substantial land-cover change and high flood risk even under the most conservative sea-level rise scenario considered, and they warrant early attention — whether through embankment reinforcement, mangrove restoration buffers, or expanded community-level early warning systems.

CONCLUSION

This study has presented an integrated, multi-year assessment of coastal vulnerability in the Indian Sundarbans, covering South 24 Parganas across 2017, 2021 and 2025 through remote sensing, GIS and DEM-based flood modelling in Google Earth Engine. Four conclusions emerge.

First, the CVI shows 31.58 percent of the study area (2,427.51 km²) fell into the High or Very High vulnerability class in 2025, with Very High alone covering 960.82 km² (12.50%), concentrated in Sagar Island, Gosaba and Patharpratima.

Second, 1,376.95 km² (17.95%) underwent a detectable land-cover shift between 2017 and 2025. The steepest change (16.13%) fell in 2017–2021, coinciding with Cyclone Amphan, while the lower 2021–2025 rate (12.62%) points to partial post-cyclone stabilisation.

Third, DEM-based flood modelling places 1,617.02 km² (21.09%) within the present-day S0 flood zone, expanding to 2,778.01 km² (36.23%) under S1 — an 82 percent increase from roughly half a metre of additional sea-level rise.

Fourth, the spatial convergence of high CVI, active land-cover change and flood risk in the southern and western blocks marks these zones as priorities for near-term coastal management and adaptation investment. Together, this assessment offers a practical, spatially explicit evidence base for more targeted coastal governance in one of the world's most climate-exposed deltas

.

REFERENCES

1) Alongi, D.M. (2008) ‘Mangrove forests: Resilience, protection from tsunamis, and responses to global climate change’, Estuarine, Coastal and Shelf Science, 76(1), pp. 1–13.

2) Anam, M.M., Al Jabir, A. and Hasan, G.M.J. (2021) ‘Bank-line behaviour of the main rivers located within Sundarbans using Digital Shoreline Analysis System’, MIST International Journal of Science and Technology, 9(1), pp. 11–21.

3) Aziz, A. and Paul, A.R. (2015) ‘Bangladesh Sundarbans: Present status of the environment and biota’, Diversity, 7(3), pp. 242–269.

4) Bandyopadhyay, S., Mukherjee, D., Bag, S., Pal, D.K. and Rudra, K. (2004) ‘20th century evolution of banks and islands of the Hugli Estuary, West Bengal, India: Evidence from maps, images and GPS survey’, in Geomorphology and Environment. Kolkata: ACB Publications.

5) Biswas, A., Mondal, S. and Ray, R. (2020) ‘InSAR-based land subsidence measurement in the Sundarbans: Implications for coastal vulnerability’, Journal of Coastal Conservation, 24(3), 44.

6) Brown, C.F., Brumby, S.P., Guzder-Williams, B. et al. (2022) ‘Dynamic World, near real-time global 10 m land use land cover mapping’, Scientific Data, 9, 251.

7) Das, A., Mondal, I., Hossain, S.K.A., Jose, F., Ouda, M.M., Juliev, M., Almaliki, A.H. and De, T.K. (2025) ‘Coastal vulnerability assessment for the Sundarbans mangrove ecosystem using InVEST and machine learning-based empirical models’, Environment, Development and Sustainability.

8) Das, T. (2021) Tidal hydrodynamics of Sundarbans estuarine system. PhD dissertation. School of

Environmental Studies, Jadavpur University, Kolkata.

9) Datta, D. and Deb, S. (2012) 'Analysis of coastal land use/land cover changes in the Indian Sunderbans using remotely sensed data', Journal of Geo-Spatial Information Science, 15(4), pp. 241–250.

10) Ganguli, B. (2024) Coastal Vulnerability Assessment, Sunderbans [Data set]. Mendeley Data, Version 1. doi: 10.17632/ckf3jk99dh.1.

11) Ghosh, M.K., Kumar, L. and Langat, P.K. (2018) 'Mapping tidal channel dynamics in the Sundarbans, Bangladesh, between 1974 and 2017, and implications for the sustainability of the Sundarbans mangrove forest', Environmental Monitoring and Assessment, 190(10), pp. 1–15.

12) Ghosh, M.K., Kumar, L. and Roy, C. (2014) 'Monitoring the coastline change of Hatiya Island in Bangladesh using remote sensing techniques', ISPRS Journal of Photogrammetry and Remote Sensing, 101, pp. 137–144.

13) Ghosh, S. and Mistri, B. (2023) 'Cyclone-induced coastal vulnerability, livelihood challenges and mitigation measures of Matla–Bidya inter-estuarine area, Indian Sundarban', Natural Hazards, 116(3), pp. 3857–3878.

14) Giri, S., Samanta, S., Mondal, P.P., Basu, O., Khorat, S., Chanda, A. and Hazra, S. (2022) 'A geospatial assessment of growth pattern of aquaculture in the Indian Sundarbans Biosphere Reserve', Environment, Development and Sustainability, 24(3), pp. 4203–4225.

15) Hale, R.P., Wilson, C.A. and Bomer, E.J. (2019) 'Seasonal variability of forces controlling sedimentation in the Sundarbans National Forest, Bangladesh', Frontiers in Earth Science, 7, 211.

16) Hazra, S. and Samanta, K. (2016) 'Temporal change detection (2001–2008): Study of Sundarban', Munich Personal RePEc Archive / IDEAS [Working paper].

17) IPCC (2022) Climate Change 2022: Impacts, Adaptation and Vulnerability. Contribution of Working Group II to the Sixth Assessment Report of the Intergovernmental Panel on Climate Change. Cambridge: Cambridge University Press.

18) Kantamaneni, K. et al. (2019) 'A systematic review of coastal vulnerability assessment studies along the Indian coast', Journal of Coastal Conservation, 23(4), pp. 883–893.

19) Kathiresan, K. and Rajendran, N. (2005) 'Coastal mangrove forests mitigated tsunami', Estuarine, Coastal and Shelf Science, 65(3), pp. 601–606.

20) Mahato, P.S. (2024) 'A study of morphological changes in the coastal areas and offshore islands of Sudarban coastline using remote sensing', IntechOpen. doi: 10.5772/intechopen.112243.

21) McLaughlin, S. and Cooper, J.A.G. (2010) 'A multi-scale coastal vulnerability index: A tool for coastal managers?', Environmental Hazards, 9(3), pp. 233–248.

22) Mukhopadhyay, A. et al. (2012) 'Automatic shoreline detection and future prediction: A case study on Puri Coast, Bay of Bengal, India', European Journal of Remote Sensing, 45(1), pp. 201–213.

23) Nandy (Datta), S. et al. (2012) 'Mangrove forest cover changes in Indian Sundarban (1986–2012) using remote sensing and GIS', School of Oceanographic Studies, Jadavpur University, Kolkata.

24) Neumann, B., Vafeidis, A.T., Zimmermann, J. and Nicholls, R.J. (2015) 'Future coastal population growth and exposure to sea-level rise and coastal flooding', PLOS ONE, 10(3), e0118571.

25) Nicholls, R.J. et al. (2021) 'Coastal sea levels and their projections', Nature Reviews Earth & Environment, 2(4), pp. 214–230.

26) Pettorelli, N., Freemantle, T.P., Fatoyinbo, T.E. and Cornforth, W.A. (2013) 'Advanced Land Observing Satellite Phased Array Type L-Band SAR (ALOS PALSAR) to inform the conservation of mangroves: Sundarbans as a case study', Remote Sensing, 5(1), pp. 224–237.

27) Rahman, M.M. et al. (n.d.) 'Delineation of decadal changes of shoreline and geomorphology over West Bengal, India using remote sensing and GIS techniques', American Geophysical Union Fall Meeting [Conference presentation].

28) Samanta, S., Hazra, S., Mondal, P.P., Chanda, A., Giri, S., French, J.R. and Nicholls, R.J. (2021) 'Assessment and attribution of mangrove forest changes in the Indian Sundarbans from 2000 to 2020', Remote Sensing, 13(24), 4957.

29) Sardar, P. and Samadder, S.R. (2021) 'Understanding the dynamics of landscape of greater Sundarban area using multi-layer perceptron Markov chain and landscape statistics approach', Ecological Indicators, 121, 106914.

30) Sarkar, S.K. et al. (n.d.) 'Assessing livelihood vulnerability to sea level rise: A perspective on climate vulnerability and adaptation in the context of the Indian Sundarbans delta', Discover Sustainability.

31) Tessler, Z.D. et al. (2015) 'Profiling risk and sustainability in coastal deltas of the world', Science, 349(6248), pp. 638–643.

32) Thieler, E.R. and Hammar-Klose, E.S. (2000) National Assessment of Coastal Vulnerability to Sea-Level Rise: Preliminary Results for the U.S. Atlantic Coast. USGS Open-File Report 99-593. Woods Hole, MA: U.S. Geological Survey.

33) West Bengal SDMA (2020) Rapid Damage Assessment Report: Cyclone Amphan, South 24 Parganas. Kolkata: Government of West Beng.